

Module Development of Multiphase and Chemically Reacting Flow in LS-DYNA[®] Compressible Flow Solver

Kyoung-Su Im, Zeng-Chan Zhang, and Grant Cook, Jr.
Livermore Software Technology Corp.
Livermore, CA 94551, USA

Abstract

We reported a significant progress of the simulation module developments such as the cavitation, supersonic heterogeneous combustion, and gaseous detonations for the compressible flow solver. The homogeneous equilibrium model (HEM) based on the acoustic speed of the mixture of liquid and vapor was implemented for automotive diesel injectors, where the cavitation effects should correctly predict for the nozzle design. The heterogeneous combustion based on an Eulerian-Lagrangian model was developed for thermobaric explosive (TBX) applications in which a stochastic particle technique in conjunction with a probability density function (PDF) is adopted. In modeling of gaseous detonation, we implemented various combustion modules depending on the reaction model: one-step reaction (ZND model), reduced reaction of intrinsic low-dimensional manifolds (ILDm), and detailed chemistry model. Application results validated with experimental data are demonstrated with detailed discussion.

Introduction

The numerical simulation of cavitating nozzle flows in high-pressure, high-speed diesel injectors has become a more widely interesting topic because the cavitation phenomenon inside a fuel injector can provide valuable and detailed information for nozzle design and spray breakup modeling. However, the numerical simulation of the cavitating flows is a difficult stiff problem accompanied from a multiphase phenomenon between liquid and gas phase. In general, there are two ways to resolve the problem. The first one is to construct an equation of state (EOS) valid for the liquid, the mixture, and the gas phase. Such a type of approach is well-posedness if one can provide a valid EOS for the mixture phase. The other is to use the non-equilibrium multiphase flow model. With this model, each phase has its own EOS and the gas phase typically by an ideal gas EOS. Many studies have tried to predict complex cavitating flows by numerical methods [1-3]. Among the existing methods, we applied Schmidt's homogeneous equilibrium model (HEM)[3], which is based on the acoustic speed of the mixture of liquid and vapor. This model is simple but contains the important characteristic information of cavitating flows. More specifically, for present diesel injection systems like a small geometry (180 μm of nozzle diameter) and very high velocities (driven by 1000-bar injection pressure through the nozzle), the continuum model considering the compressibility of the liquid and vapor should be able to correctly predict the cavitating effects from two different nozzle geometries, which would be able to more clearly understand the near nozzle breakup and sprays.

Heterogeneous combustion (i. e, solid and gas or liquid and gas) has a wide range of applications such as solid rocket propulsion, controlling the combustion instability, underwater explosion, and high energy explosion [4-6]. Among several possible combinations, a thermobaric explosive (TBX) composed of trinitrotoluene (TNT) and energetic metal particles (typically aluminum) is a widely used explosive and is of great importance in the safety, mining, and defense industries. After the onset of the detonation developed from the initial burst charge, TBX is typically accompanied by a secondary combustion, or afterburning, which releases more energy than the initial bursting charge explosion so that a fairly large combustion area within the fireball radius is sustained until all combustion products are consumed [7].

In general, there are three experimental methods to initiate detonation: (i) flame initiation, (ii) shock wave initiation, and (iii) direct initiation. In all three cases, shock waves occur prior to detonation initiation. The present paper demonstrates on the third initiation mode, which is relevant to the detonation initiation process in a pulse detonation engine (PDE). In this mode [8-10], a large amount of energy is instantaneously deposited to a small region of unconfined combustible mixture. Immediately, a strong blast wave is generated. This spherical (or cylindrical) shock wave expands and decays while it continues heating the gas mixture. Due to shock heating, chemical reactions occur and chemical energy is released. Under suitable conditions, detonation is initiated. The blast wave generated by igniter plays an important role because it produces the critical states for the onset of the detonation. For the present demonstration, three initiation energies are used for the supercritical, the sub-critical, and the critical processes and a realistic finite-rate chemistry model is used for the H₂/O₂/Ar premixed mixture.

Since cavitating flow and chemical reacting flows are highly transient and very stiff problems, the numerical method adapted must be time-accurate and robust to accommodate complex phenomena. To resolve the difficulties, the space-time conservation element and solution element (CE/SE) method [11] is employed. Most importantly, the CE/SE method is substantially different in both concept and methodology from the traditional computational fluid dynamics (CFD) methods, which is now available in LS-DYNA[®] compressible solver.

Model Equation

Cavitation Equation

The equation system governing the high speed cavitating flow is given by,

$$\frac{\partial \bar{u}}{\partial t} + \frac{\partial F(\bar{u})}{\partial x} + \frac{\partial G(\bar{u})}{\partial y} + \frac{\partial H(\bar{u})}{\partial z} = \frac{\partial F_v(\bar{u})}{\partial x} + \frac{\partial G_v(\bar{u})}{\partial y} + \frac{\partial H_v(\bar{u})}{\partial z} \quad (1)$$

where, t is time, x and $y > 0$ are the axial and radial-direction coordinates, \bar{u} is the primitive flow variable vector, $F(\bar{u})$, $G(\bar{u})$, and $H(\bar{u})$ are flux vectors, $F_v(\bar{u})$, $G_v(\bar{u})$, and $H_v(\bar{u})$ are viscous flux vectors, respectively. Details about the flux vector and viscous flux can be found in [3].

The gas phase EOS was used by an ideal gas equation. When the speed of sound is given, the EOS for the mixture is driven by integrating an isentropic relation ($dp = a^2 d\rho$, where, a is a speed of sound) from the saturated liquid state to a state existing the mixture phase and such a EOS is given by,

$$p = p_l^{sat} + \frac{\rho_g a_g^2 \rho_l a_l^2 (\rho_g - \rho_l)}{\rho_g^2 a_g^2 - \rho_l^2 a_l^2} \cdot \log \left\{ \frac{\rho_g a_g^2 [\rho_l + \alpha(\rho_g + \rho_l)]}{\rho_l (\rho_g a_g^2 - \rho_l a_l^2)} \right\} \quad (2)$$

where, p_l^{sat} is the saturation pressure, and α is the void fraction. The subscripts represent the corresponding the gas, g and liquid, l phase, respectively. The void fraction, α is defined as,

$$\alpha = \frac{\rho - \rho_l}{\rho_g - \rho_l} \quad (3)$$

Since all parameters except the void fraction are given by the fluid properties, the EOS of the mixture phase is the function of the mixture density, ρ only. The pure liquid phase of EOS can be also obtained by using the isentropic relation combined with saturation pressure as,

$$p = p_l^{sat} + a_l^2 \rho \quad (4)$$

Reacting Flow Equation

The governing equations for the 3-D unsteady, multi-species reactive Euler equations are given by,

$$\frac{\partial u_m}{\partial t} + \frac{\partial f_m^x}{\partial x} + \frac{\partial f_m^y}{\partial y} + \frac{\partial f_m^z}{\partial z} = S(u_m) + W(u_m), \quad m=1,2,3,\dots,n_s+5 \quad (5)$$

where t , x , y , and z are the time, x-, y-, and z-direction coordinates, respectively. u_m , f_m^x , f_m^y , and f_m^z , $m=1,2,3,\dots,n_s+5$ are the primitive flux-vector variables corresponding to x-, y-, and z-direction flow.

$$\begin{aligned} u_m &= [\rho, \rho u, \rho v, \rho w, E_t, \rho y_1, \dots, \rho y_{n_s}]^T \\ f_m^x &= [\rho u, \rho u^2 + p, \rho uv, \rho uw, (E_t + p)u, \rho u y_1, \dots, \rho u y_{n_s}]^T \\ f_m^y &= [\rho v, \rho vu, \rho v^2 + p, \rho vw, (E_t + p)v, \rho v y_1, \dots, \rho v y_{n_s}]^T \\ f_m^z &= [\rho w, \rho wu, \rho wv, \rho w^2 + p, (E_t + p)w, \rho w y_1, \dots, \rho w y_{n_s}]^T \end{aligned} \quad (6)$$

where, ρ , u , v , w , p , and E_t are the mass density, x-velocity component, y-velocity component, z-velocity component, static pressure, and the total energy per unit volume of the gas mixture, respectively and $y_k = \rho_k / \rho$, $k=1,2,\dots,n_s$ (where, ρ_k is the mass density of species k , and n_s is number of species involved) are mass fraction of species k . The total energy E_t per unit volume can be expressed as

$$E_t = \rho \left(e + \frac{1}{2} u_i u_i \right), \quad i = x, y, z \quad (7)$$

where $e = \sum_{k=1}^{n_s} y_k e_k$, is the specific internal energy of the mixture and e_k is the specific internal energy of species k . From the thermodynamics relation, the specific internal energy for the mixture can be expressed as

$$e = h - \frac{p}{\rho} = \sum_{k=1}^{n_s} y_k h_k - \frac{p}{\rho}, \quad (8)$$

where h is the specific enthalpy of the mixture, and $h_k = \int_{T_{ref}}^{def} c_{pk} dT + h_{fk}$ is the specific enthalpy of species k . c_{pk} , $k=1,2,\dots,n_s$ are the specific heat coefficients at constant pressure given by an available database in Ref. [12]. By using Eq. (8), it is not necessary to add the heat of combustion due to reactions in the energy equation as a source term, but the temperature should be backed out by solving a nonlinear equation.

The $S(\bar{u})$ is the coupling source term vector due to solid metal particles, and $W(\bar{u})$ the chemical reacting source term vector described as,

$$\begin{aligned} S(u_m) &= [s_1, s_2, s_3, s_4, s_5, \dots, s_k, \dots]^T \\ W(u_m) &= [0, 0, 0, 0, 0, \rho \Omega_1, \dots, \rho \Omega_{n_s}]^T \end{aligned} \quad (9)$$

where s_1 , s_2 , s_3 , s_4 , s_5 , and s_k are the exchange terms representing the mass, x-momentum, y-momentum, z-momentum, total energy, and k -th species for the vapor generation. Detailed description about particle source term can be found in [13].

The components, $\rho\Omega_k = W_k\dot{\omega}_k$, $k=1,2,\dots,n_s$ (where W_k is the molecular weight and $\dot{\omega}_k$ is the net molar production rate of species k) in the chemical source term vector are the total production rate of the species k . For a system of reacting gases, a detailed mechanism of elementary reactions is required to evaluate the source terms as

$$\sum_{k=1}^{n_s} v'_{kl} X_k \rightleftharpoons \sum_{k=1}^{n_s} v''_{kl} X_k, \quad l=1,\dots,n_q \quad (7)$$

where v'_{kl} and v''_{kl} are the forward and backward stoichiometric coefficients, respectively. X_k is the chemical symbol of the species k , and n_q is the total number of reactions in the mechanism. Then, the net molar production rate of species k can be expressed as

$$\dot{\omega}_k = \sum_{l=1}^{n_q} (v'_{kl} - v''_{kl}) \left[k_{fl} \prod_{k=1}^{n_s} [X_k]^{v'_{kl}} - k_{bl} \prod_{k=1}^{n_s} [X_k]^{v''_{kl}} \right], \quad (8)$$

where k_{fl} and k_{bl} are the forward and backward rate coefficients of reaction l , respectively, and $[X_k]$ is the concentration of species k . The rate coefficients are typically given in Arrhenius form.

$$k_{fl} = A_l T^{\beta_l} \exp\left(-\frac{E_{al}}{RT}\right) \quad (9)$$

where A_l is the pre-exponential factor, β_l is the temperature exponent, E_{al} is the activation energy per unit mole, T is the temperature, and R is the universal gas constant.

For a system of the ideal gases, the equation of state is given as,

$$p = \rho R_g(y_k) T(e, y_k) \quad (10)$$

R_g is the gas constant for the mixture and given by,

$$R_g(y_k) = \frac{R}{W(y_k)} = R \sum_{k=1}^{n_s} \frac{y_k}{W_k} \quad (11)$$

where W is the mean molar mass of the mixture.

Particle Equation

For a dilute solid flow in a Lagrangian reference frame, a computational particle represents a finite number of particles having the same diameter, velocity, and temperature. Then, the particle position is given by

$$\frac{dx_{p,i}}{dt} = u_{p,i}, \quad i = x, y, z \quad (12)$$

The rate of particle mass, momentum, and energy change is given by enforcing the conservation law of an individual particle.

$$\begin{aligned} \frac{dm_p}{dt} &= \frac{d}{dt} \left(\frac{4}{3} \pi \rho_p r_p^3 \right) = -\dot{m}_p \\ m_p \frac{du_{p,i}}{dt} &= m_p g_{p,i} + D_p(u_i)(u_i - u_{p,i}), \quad i = x, y, z \\ m_p c_p \frac{dT_p}{dt} &= \dot{m}_p L(T_p) + 4\pi r_p^2 \dot{q}_p \end{aligned} \quad (13)$$

where $g_{p,i}$, $i = x, y, z$, is the particle gravity exerted in x-, y-, and z-direction. $D_p(u_i)$ is the drag function and is given by

$$D_p(u_i) = 0.5\pi r_p^2 \rho C_D |u_i - u_{p,i}|, \quad i = x, y, z \quad (14)$$

where C_D is the drag coefficient, typically determined by an empirical relation. $L(T_p)$ is the heat of vaporization of the aluminum particle, and \dot{q}_p is the rate of heat transfer by conduction and radiation to the particle surface per unit area.

$$\dot{q}_p = \dot{q}_{rad} + \dot{q}_{cond} = \varepsilon \sigma_b (T^4 - T_p^4) + \frac{k_g(T)}{2r_p} (T - T_p) Nu_p \quad (15)$$

where ε is the emissivity of the aluminum particle, σ_b ($= 5.6703e^{-8} \text{ J/m}^2 \cdot \text{K}^4 \cdot \text{s}$) the Stefan-Boltzmann constant, and $k_g(T)$ the heat conduction coefficient as a function of temperature averaged over the gas and solid particle. Nu_p is the Nusselt number given by

$$Nu_p = 2 + 0.67 pr^{1/3} Re_p^{1/2}, \quad Re_p = \frac{2r_p |u_i - u_{p,i}| \rho}{\mu} \quad (16)$$

where Re_p is the particle Reynolds number evaluated with a relative velocity.

Since the ignition and burning rate of metal particles are directly related to the different particle sizes, we selected both a mono-dispersed and a poly-dispersed distribution such as the Rosin-Rammler probability density function, where the particles are distributed by referencing an average radius.

$$f(D) = 1 - \exp\left(-\frac{D^{3.5}}{\bar{D}}\right) \quad (17)$$

where \bar{D} is the average diameter.

Results and Discussion

Figure 1(a-f) shows a typical single hole diesel nozzle visualized by X-ray phase contrast imaging technique and a snapshot of internal cavitating flows for different geometries. Clearly, the flow inside a non-hydroground nozzle shows very strong cavitation while the hydroground nozzle generates only weak cavitating flow, which provides a clear evidence of the geometrical effect. To further illustrate the geometrical effects, the velocity components of axial and vertical direction were integrated along with the nozzle cross-sectional axis and taken their average values (u_x and u_y). Next, by defining an axial coordinate (x/D), which is normalized by the nozzle diameter D and set the origin at the nozzle inlet (see Fig. 1c and e), the velocity ratio (u_x/u_y) is calculated along that axis and the interesting areas of near nozzle exit ($x/D = 3.5$ to 4.5) are plotted in Fig. 1d and f to visualize the diverging flow angle. The velocity ratio of the hydroground nozzle shows almost constant indicating that the flow is not enough to widen the spray into the chamber. On the other hand, the comparable diverging flow angle (3°) is clearly obvious in the nonhydroground nozzle, indicating that the spray cone angle is caused by the cavitation inside the nozzle.

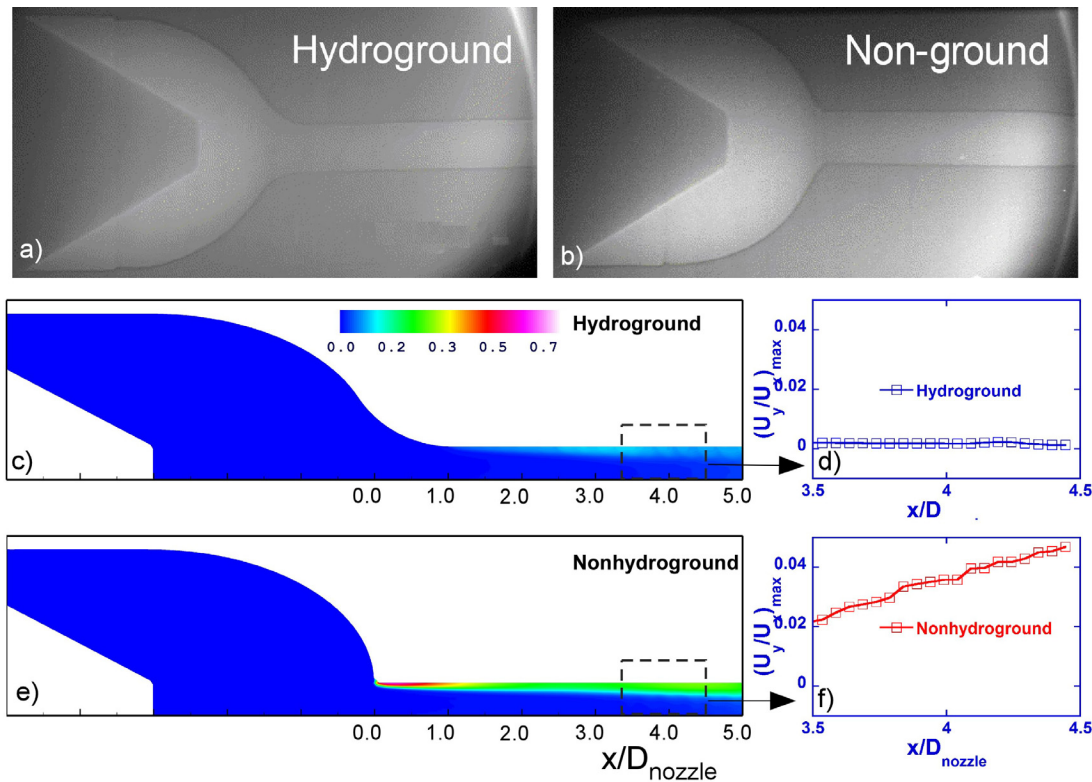


Fig. 1 Comparisons of cavitating flows for nonhydroground and hydroground inlet with the velocity ratio comparisons in axial and perpendicular direction along axial position close to the exit of the orifice. The coordinate origin is located at the inlet of the nozzle with a dimensionless variable $x/D=0$, using nozzle diameter D , and the nozzle exit is at $x/D=5$.

Figure 2 shows the schematics of the experimental chamber and an initial charge of TBX. The closed bomb test (CBT) chamber has a dimension of 40 cm in radius (r,y,z) and 150cm in longitudinal length so that the total volume of the chamber is 0.754 m^3 . Two pressure gauges (Kulite; HEL-375-250A, and HEL-375-500A) having different sensing capacities were installed, the one at the front center of the cylinder ($x=75\text{cm}$, $r=40\text{cm}$) and the other at the side center of the cylinder base surface ($x=150\text{cm}$, $r=0\text{cm}$), respectively. The measured pressure data from the sensors were logged by the data acquisition system, DEWE-500, for analysis of the blast performance. The cylindrical (30 mm in diameter and 33mm in length) Tritonal TBX charge weighs 40 g and consists of well mixed TNT (80%) and aluminum particles (20%, with an average diameter of $10 \mu\text{m}$). The main charge, combined with the blast cap (5g booster explosives of TNT compounds) and the exploding bridge wire (EBW) shown in Fig. 2b was initially located at the CBT center ($x=75\text{cm}$, $r=0\text{cm}$) of the CBT chamber for each experiment. Several experiments were conducted to obtain reliable data sets, and three data sets were collected with less than 10 % standard relative error (SRE) from the average at each time instant. Also shown are the TBX validations with the pressure data sets for the side and front center position between the simulation results and averaged experimental data. Fig. 2c and d illustrate the pressure history at the side and front center, respectively, and Fig. 2e and f show the corresponding impulse, which is defined as pressure integrated over time.

When the blast waves arrives at the side center, the pressure immediately peaks to its maximum value, and the reflected wave from the cylinder wall results in the subsequent peaks as the process repeats, conjugates, and dissipates until the pressure converges to an elevated value, but still with considerably noisy patterns after 5ms from the initial explosion. This phenomenon

as shown in Fig. 2d is more obvious at the front center location. Integrating the pressure with time, the corresponding impulses are smoother and gradually increasing, with very similar profiles both at the side and the front center locations. The only distinguishable patterns are detected for the earlier time period with more dynamic impulse acting on the side center, as shown in the magnified boxes in the Figures. It is clear that the simulation results are in excellent agreement with the experimental data over the time ranges.

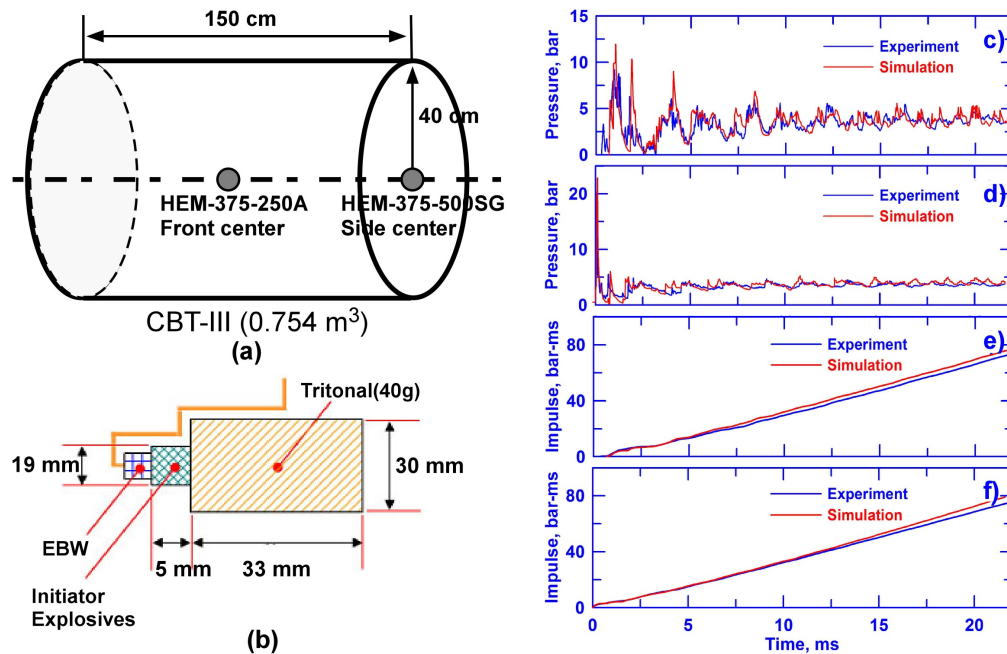


Fig. 2 Experimental set up for the TBX flow in closed bomb chamber: a) and b) and comparisons between measured data and simulation at the side and front center positions: c) and d) are the pressure histories, e) and f) are the impulses versus time.

Figure 3 shows the simulation results of three regimes of direct initiation according to different initiation energy. The ratio of local maximum pressure to initial reactant pressure is plotted as a function of the radial locations of the leading shock wave. For reference, the pressure of the von-Neuman spike of the corresponding self sustained CJ detonation (for the driven section) is also plotted by dot line. In a series of calculations by incrementally increasing the values of the deposited initiation energy, the three regimes can be clearly observed. When the initial energy $E_s = 33.0 \text{ J/cm}$, the strong blast wave decays to a wave with peak pressures much lower than the CJ value, indicating a failed detonation initiation process. Two initial energies of $E_s = 43.0 \text{ J/cm}$ and $E_s = 53.0 \text{ J/cm}$ are in the critical regime. Distinct pressure peaks are observed. The deposited initiation energies are not high enough to sustain stable detonation waves. This unstable period ends at $R = 30\text{cm}$, and the waves become the self-sustained CJ detonation waves. With higher initiation energy for $E_s = 76.3 \text{ J/cm}$, the initial blast wave directly initiate the detonation wave, which expands and decays to the CJ value with mild instabilities. The corresponding experimental schlieren images are also illustrated in the figure.

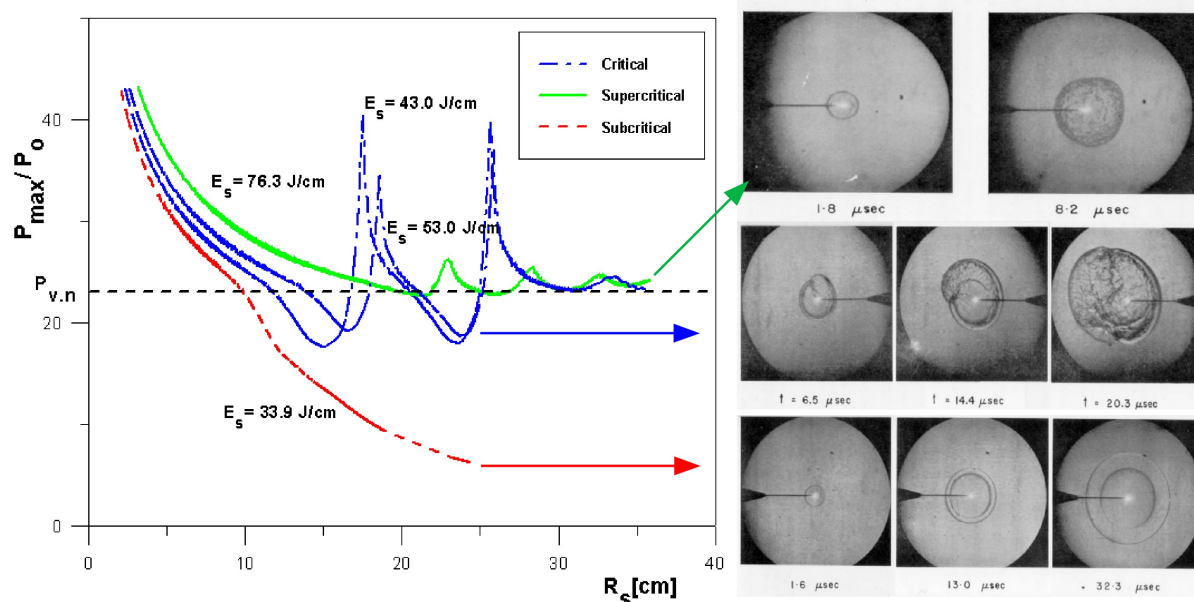


Fig. 3 The spatial histories of local maximum pressures in the three regimes of direct initiation processes of a cylindrical detonation in a $2H_2 + O_2 + 7Ar$ mixture.

References

- [1] Kubota, A, Kato, H, Yamaguchi, H, and Maeda, M., *J of Fluids Eng.* 11:204-210 (1989).
- [2] Chen, Y., Heister, S.D., *Computers & Fluids.* 24, 7, 799-809 (1995).
- [3] Schmidt, D.P., Rutland, C. J., Corradini, M. L., *Atomization Sprays Technology* 9:255-276 (1999).
- [4] E.W. Price, K.J. Kraeutle, J.L. Prentice, T.L. Boggs, J.E. Crump, and D.E. Zurn, *Behavior of Aluminum in Solid Propellant Combustion*, NWC TP 6120 (1982).
- [5] J. Massoni, R. Saurel, A. Lefrancois, and G. Baudin, *Shock Waves*, 16:75-92 (2006).
- [6] K. Kim, W. Wilson, J. Colon, T. Kreitingner, C. Needham, et.al, WIT Transaction on The Built Environment, Vol 87 (2006).
- [7] D. Schwer and K. Kailasanath, Technical Report NRL/MR/6410-02-8636 (2002).
- [8] I. B. Zel'dovich, S. M. Kogarko, and N. N. Simonov, *Sov. Phys. Tech. Phys.* 1(8), pp. 1689-1713 (1956).
- [9] G. G. Bach, R. Knystautas, and J. H. Lee, *12th Symp. Int. Combust. Proc.*, pp. 853-867 (1969).
- [10] K.-S. Im, and S.-T. J. Yu, AIAA-2003-1318 the 41th Aerospace Sciences Meeting and Exhibit, Reno, NV (2003).
- [11] Z.-C. Zhang, S.-T. Yu, and S.-C. Chang, *Journal of Computational Physics*, (2002) 175: 168-199.
- [12] S. Gordon and B.J. McBride, Computer Program for Calculation of Complex Chemical Equilibrium Compositions, Rocket Performance, Incident and Reflected Shocks, and Chapman-Jouguet Detonations, NASA SP-273, 1976.
- [13] K.-S. Im, C.-K. Kim, Z.-C. Zhang, and Grant Cook, Jr., submitted in *33rd Proc. Combust. Institute*, (2010).